INTERNATIONAL JOURNAL OF CLIMATOLOGY
Int. J. Climatol. **26**: 1937–1956 (2006)
Published online 4 May 2006 in Wiley InterScience
(www.interscience.wiley.com) DOI: 10.1002/joc.1343

RMetS
ROYAL METEOROLOGICAL SOCIETY

INTERANNUAL VARIABILITY OF THE TROPICAL ATLANTIC INDEPENDENT OF AND ASSOCIATED WITH ENSO: PART I. THE NORTH TROPICAL ATLANTIC

ITSUKI C. HANDOH,[a,*] ADRIAN J. MATTHEWS,[a,b] GRANT R. BIGG[c] and DAVID P. STEVENS[b]

[a] *School of Environmental Sciences, University of East Anglia, Norwich, UK*
[b] *School of Mathematics, University of East Anglia, Norwich, UK*
[c] *Department of Geography, University of Sheffield, Sheffield, UK*

Received 26 April 2005
Revised 17 November 2005
Accepted 3 March 2006

ABSTRACT

The interannual variability of the tropical Atlantic ocean–atmosphere system is examined using 50 years of sea-surface temperature (SST) and re-analysis data, and satellite data when available. A singular value decomposition analysis of 12- to 72-month bandpass filtered SST and zonal wind stress reveals two dominant modes of interannual variability. The SST anomalies are confined to the North Tropical Atlantic (NTA) in the first mode and extend over the equatorial and South Tropical Atlantic in the second mode. No evidence is found for an Atlantic SST dipole. The structure of the first (NTA) mode is examined in detail here, while the second mode has been described in a companion paper. In particular, the relationship of the NTA mode with El Niño–Southern Oscillation (ENSO) is investigated. There are 12 NTA events (seven warm and five cold) that are associated with ENSO, and 18 NTA events (seven warm and 11 cold) that are independent of ENSO.

The ENSO-associated NTA events appear to be a passive response to remote ENSO forcing, mainly via a Pacific-North America (PNA)-like wave train that induces SST anomalies over the NTA through changes in the surface wind and latent heat flux. The NTA anomalies peak four months after ENSO. There does not appear to be an atmospheric response to the NTA SST anomalies as convection over the Atlantic is suppressed by the anomalous Walker circulation due to ENSO.

The ENSO-independent NTA events also appear to be induced by an extratropical wave train from the Pacific sector (but one that is independent of Pacific SST), and forcing by the North Atlantic Oscillation (NAO) also contributes. As the event matures, the atmosphere does respond to the NTA SST anomalies, with enhanced convection over the Caribbean and a wave train that propagates northeastward to Europe. Copyright © 2006 Royal Meteorological Society.

KEY WORDS: tropical atlantic variability; ENSO; ocean–atmosphere interaction; teleconnections; North Atlantic Oscillation

1. INTRODUCTION

Interannual variability in the tropical Atlantic is more complex than in the Pacific where El Niño–Southern Oscillation (ENSO) is the single dominant mode of variability. Equatorial warm events, analogous to ENSO, do occur in the Atlantic (Zebiak, 1993) with a quasi-biennial signature (Tourre *et al*., 1999; Tseng and Mechoso, 2001; Mo and Häkkinen, 2001). These equatorial warm events are maintained by a Bjerknes-type feedback involving ocean dynamics (Hirst, 1988; Xie *et al*., 1999), although their amplitude is much less than in ENSO events in the Pacific.

The tropical Atlantic also exhibits coherent off-equatorial variability. On decadal timescales, sea-surface temperature (SST) anomalies tend to be antisymmetric north and south of the equator, leading to a tropical dipole mode (Chang *et al*., 1997; Huang and Shukla, 1997; Okumura *et al*., 2001). However, SST anomalies

* Correspondence to: Itsuki C. Handoh, Department of Applied Mathematics, The University of Sheffield, The Hicks Building, Hounsfield Road, Sheffield S3 7RH, United Kingdom; e-mail: i.handoh@shef.ac.uk

Copyright © 2006 Royal Meteorological Society

WILEY InterScience® DISCOVER SOMETHING GREAT

north and south of the equator are not anti-correlated, and the existence of the dipole mode is disputed (Houghton and Tourre, 1992; Dommenget and Latif, 2000; Mo and Häkkinen, 2001). The off-equatorial variability appears to be maintained by anomalous air–sea fluxes through a Wind–Evaporation–SST (WES) feedback (Xie and Philander, 1994), while ocean dynamics are of secondary importance (Carton *et al*., 1996). The WES feedback appears to be at work on inter-decadal timescales, but the interannual analogue to this may be more a manifestation of SST response to the atmospheric wind anomalies; no two-way ocean–atmosphere feedback has been confirmed (Czaja *et al*., 2002) or perhaps only a weak positive feedback occurs over the deep tropics (Joyce *et al*., 2004).

Hence, there appears to be two primary modes of variability in the tropical Atlantic on interannual timescales: (1) a North Tropical Atlantic (NTA) mode, (2) variability along the equator, which extends into the South Tropical Atlantic by a coastal Kelvin wave that propagates southward along the African coast, generating westward-propagating Rossby waves (Handoh and Bigg, 2000). Together, this constitutes a South Tropical Atlantic (STA) mode (e.g. Enfield and Mayer, 1997).

Approximately half of the variance of tropical Atlantic SST variability on interannual timescales is driven by remote forcing (Liu *et al*., 2004), with ENSO and the North Atlantic Oscillation (NAO) being the major drivers (Saravanan and Chang, 2000; Sutton *et al*., 2000, 2001; Huang *et al*., 2002; Czaja *et al*., 2002; Chang *et al*., 2003). For example, warm events in the tropical Atlantic were triggered by the preceding El Niño events in the Pacific in 1984 (Delecluse *et al*., 1994) and 1998 (Elliott *et al*., 2001; Curtis *et al*., 2001). These events tend to be locked to the annual cycle, with ENSO peaking in the northern autumn and winter, and the Atlantic SSTs peaking in the following spring (Sutton *et al*., 2000; Enfield and Mayer, 1997; Mo and Häkkinen, 2001). The link appears to be both via extratropical wave trains, the Pacific–North American (PNA) pattern in the Northern Hemisphere (Lau and Nash, 1996), and the Pacific–South American (PSA) pattern in the Southern Hemisphere (Mo and Häkkinen, 2001), and by changes to the tropical Walker circulation through an atmospheric equatorial Kelvin wave (Sutton *et al*., 2000). However, the tropical Atlantic does appear to exhibit variability that is independent from external forcing (Carton and Huang, 1994) and may undergo a self-sustained ocean–atmosphere coupling (Handoh and Bigg, 2000).

In this paper we further investigate the NTA and STA modes of interannual variability in the tropical Atlantic and analyse the events that occur independently of ENSO separately from the events that are associated with ENSO over the 1–6 year band, focusing on the ocean–atmosphere interactions and time evolution for each type of event. We present an overview of the analysis and detailed results for the NTA mode. The detailed results for the STA mode will be described in a companion paper (Handoh *et al*., 2006). It is worth noting that there is significant decadal-scale variability in the tropical Atlantic as well (e.g. Mehta, 1998), as we confirmed with a power spectrum analysis of 12-month low-pass filtered data, which revealed distinct peaks over 1–5 and 8–15 year bands. However, here we are only considering the higher frequency interannual variability.

2. DATA AND ANALYSIS

2.1. Data

We used monthly mean sea-surface temperature (SST), surface zonal (τ_x) and meridional (τ_y) wind stress, and sea-level pressure (SLP) in order to examine the surface structure of the climate variability, zonal and meridional wind components, horizontal divergence and stream function at three different pressure levels: 1000, 850, and 200 hPa. The pressure coordinate vertical velocity at 500 hPa is also used. The SST data were from the UK Met Office Global Ice and Sea-Surface Temperature (GISST) data set and the remaining variables were from the National Centers for Environmental Prediction–National Center for Atmospheric Research (NCEP–NCAR) re-analysis (Kistler *et al*., 2001). We used the period from January 1948 to December 1999.

We have shorter sets of monthly mean data of outgoing longwave radiation (OLR; Liebmann and Smith, 1996), surface shortwave radiation flux, surface longwave radiation flux, latent heat flux, and sensible heat flux. OLR was used as a proxy for deep tropical convection for the period 1974–1999. The latent and sensible heat fluxes were calculated using the Tropical Ocean Global Atmosphere–Coupled Ocean Atmosphere Response Experiment (TOGA–COARE) bulk flux algorithm (Fairall *et al*., 1996) with daily SST and surface

Copyright © 2006 Royal Meteorological Society

DOI: 10.1002/joc

atmospheric data sets as input parameters from July 1983 to June 1999; these were then averaged to produce monthly means. We employed the International Satellite Cloud Climatology Project (ISCCP) D2 monthly data to calculate shortwave and longwave radiation fluxes. The algorithms for these radiation flux estimates are adapted from Bishop and Rossow (1991) and Gupta *et al*. (1992), respectively. This provides independent estimates of shortwave and longwave radiation fluxes from those of the NCEP-NCAR re-analysis. Owing to the limited vertical pressure levels of the Television Infrared Observation Satellite Program–Operational Vertical Sounder (TIROS–TOVS) data in ISCCP D2 products, we used linear interpolation (Darnell *et al*., 1983) to estimate TOVS-derived temperature and water burden at each 50 hPa interval.

The SST, shortwave, and longwave radiation data were interpolated onto a $2.5^\circ \times 2.5^\circ$ grid to match the spatial resolution of the NCAR-NCEP re-analysis data sets. We removed the long-term linear trend and annual cycle from each data set, and then applied an order 12 Butterworth filter to derive interannual fluctuations in the 12- to 72-month (1–6 year) band. We have chosen this band width because the recognised quasi-periodicity of interannual climate variability in the tropical Atlantic falls within it (Tourre *et al*., 1999; Mo and Häkkinen, 2001), while quasi-decadal variability over the basin has also been reported (Mehta, 1998). With this 1–6 year band, we will be able to address the linkages between the tropical Atlantic variability and ENSO. Owing to the filter, the first and last 12 months of data were removed.

2.2. Singular value decomposition analysis

Singular value decomposition (SVD) analysis (Bretherton *et al*., 1992) was used to determine the zero-lagged coherent spatio-temporal structure of SST and τ_x anomalies. Each field was normalised prior to calculating a covariance matrix. We have adopted SVD analysis because it maximises the explained covariance between the two fields. The SVD analysis also allows us to determine the temporal variation of the coupling strength between the two fields (see below), separating some coupled events from the rest. The spatial domain used for this analysis is the tropical Atlantic ocean, including its regional basins, from 30 °S to 30 °N (Figure 1(a)).

The output of the SVD analysis consists of spatial patterns and a paired time series for SST and τ_x anomalies (Figure 1) for each mode. The correlation coefficient between the two time series is indicative of the extent of coupling between them. It should, however, be stressed that this 'data coupling' does not necessarily indicate the existence of physical coupling between SST and τ_x anomalies. Therefore, we will examine the possible physical coupling and feedback of each SVD mode later in Section 2.2.

Modes 1 and 2 explain 48% and 30%, respectively, of the covariance of SST and zonal wind stress, and are well separated from the higher modes. The spatial structure of the SST anomaly in mode 1 (Figure 1(a)) can be identified as the NTA pattern, similar to the SST-based second rotated Empirical Orthogonal Function (EOF) mode of Enfield and Mayer (1997). Large positive SST anomalies extend from the Caribbean eastward towards West Africa with a weak signal of opposite sign to the north. This could be part of the so-called NAO tripole pattern discussed in Section 3.1. Towards the equator and the southern tropical Atlantic, the anomalies are weaker and provide a meridional SST anomaly gradient, which is a characteristic of the meridional mode.

The corresponding τ_x anomaly pattern (Figure 1(b)) is dynamically linked to that of SST. Westerly wind stress anomalies over the northern tropical Atlantic would reduce the climatological wind stress due to the trade wind easterlies, and lead to an increase in SST through a reduction in the latent heat flux.

Mode 2 displays the largest, organised signals in both SST and τ_x anomalies over the southern tropical Atlantic (Figure 2(a) and (b), respectively), consistent with the STA pattern of Enfield and Mayer (1997) and Mo and Häkkinen (2001). Modest, isolated anomalies exist over the western tropical North Atlantic basin. The largest positive τ_x anomalies are located west of the SST anomalies, with weak, negative anomalies of τ_x to the east of the SST anomaly maximum.

These two leading SVD modes of coherent SST-τ_x anomalies show the reverse order of explained variance to Enfield and Mayer's (1997) SST-based rotated EOF modes, but to similar levels of variance explained for the two modes combined. We suggest that ocean–atmosphere co-variability is more pronounced in the NTA mode than in STA. Like Chang *et al*. (2000), we also performed SVD analysis of SST and both components of surface wind stress (τ_x, τ_y). The results were almost identical to the original analysis of SST-τ_x anomalies.

Copyright © 2006 Royal Meteorological Society

DOI: 10.1002/joc

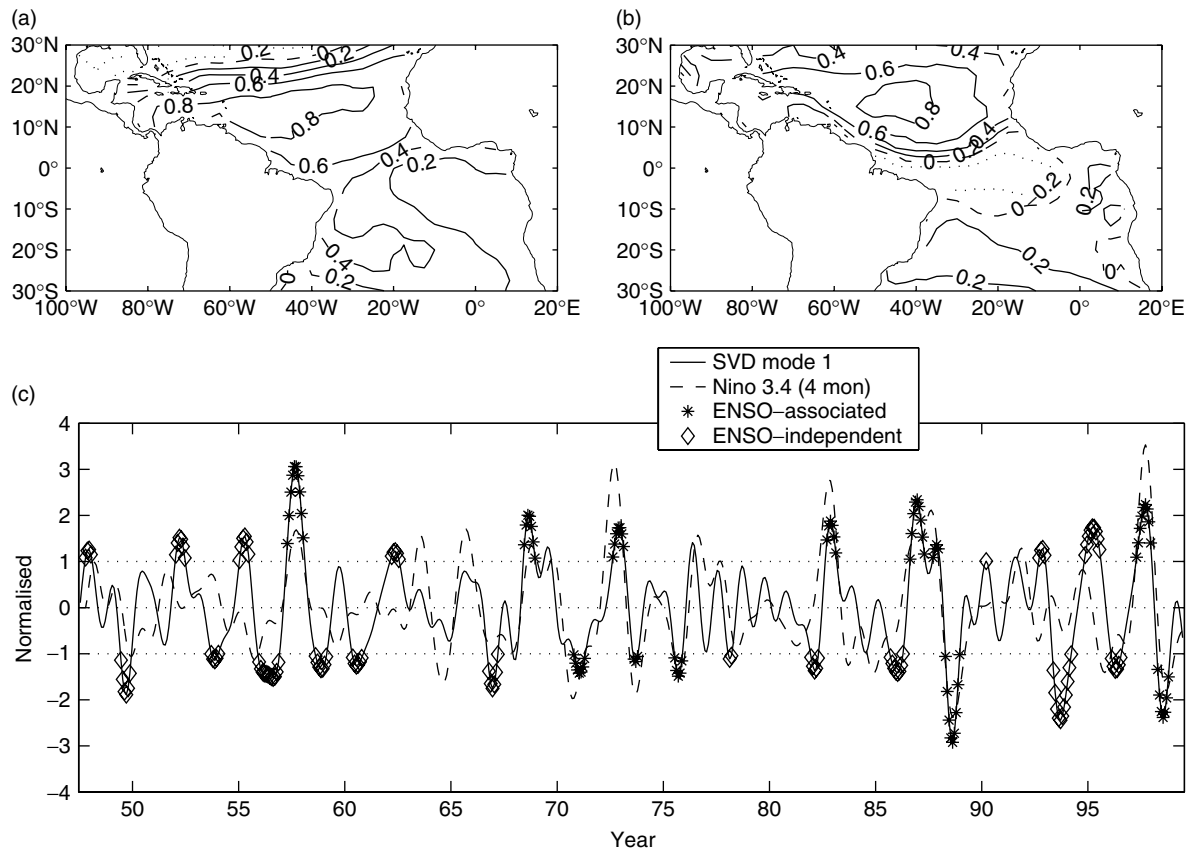

Figure 1. Anomaly correlation maps of SVD 1 over the Atlantic domain (30 °S–30 °N), (a) SST anomaly, (b) zonal wind stress anomaly. Contour interval is 0.2. Negative contours are dotted, and the zero contour is dashed. (c) Time series of A1 (solid line) and NINO3.4 lagged by 4 months (dashed line). Months included in the ENSO-associated and ENSO-independent composites are indicated by stars and diamonds, respectively

This suggests that on interannual timescales (1–6 year band), the zonal component of the wind stress vectors is the key variable that co-varies with SST, whatever the mode. It should, however, be stressed that different conclusions may occur if decadal time scales are considered. For simplicity, we have used the SVD analysis of SST-τ_x for this study of the interannual variability.

We also performed SVD analyses for four individual seasons: December–January–February (DJF), March–April–May (MAM), June–July–August (JJA), and September–October–November (SON). There is no pronounced seasonal dependency in the spatial patterns of the tropical Atlantic ocean–atmosphere variability; the seasonal patterns are very similar to the all-year round patterns shown in Figures 1 and 2. There is no indication of a distinct tropical Atlantic SST dipole pattern in any season. Therefore, noting that the difference in the amplitude of each mode from one season to another appears in the magnitude of the corresponding time series, we employ SVD outputs derived from the full seasonal cycle. However, it should be stressed that the interannual variability in the tropical Atlantic SST anomalies linked to ENSO could depend on the seasonal background, as described by Sutton *et al*. (2000). We will discuss the seasonal variability where appropriate, with emphasis on mid-latitude dynamics.

2.3. Composite analysis

An in-phase relationship between the SST and τ_x time series for each SVD mode is indicative of strong data coupling, but it does not necessarily mean dynamical and thermodynamical coupling. Both modes show

Copyright © 2006 Royal Meteorological Society

DOI: 10.1002/joc

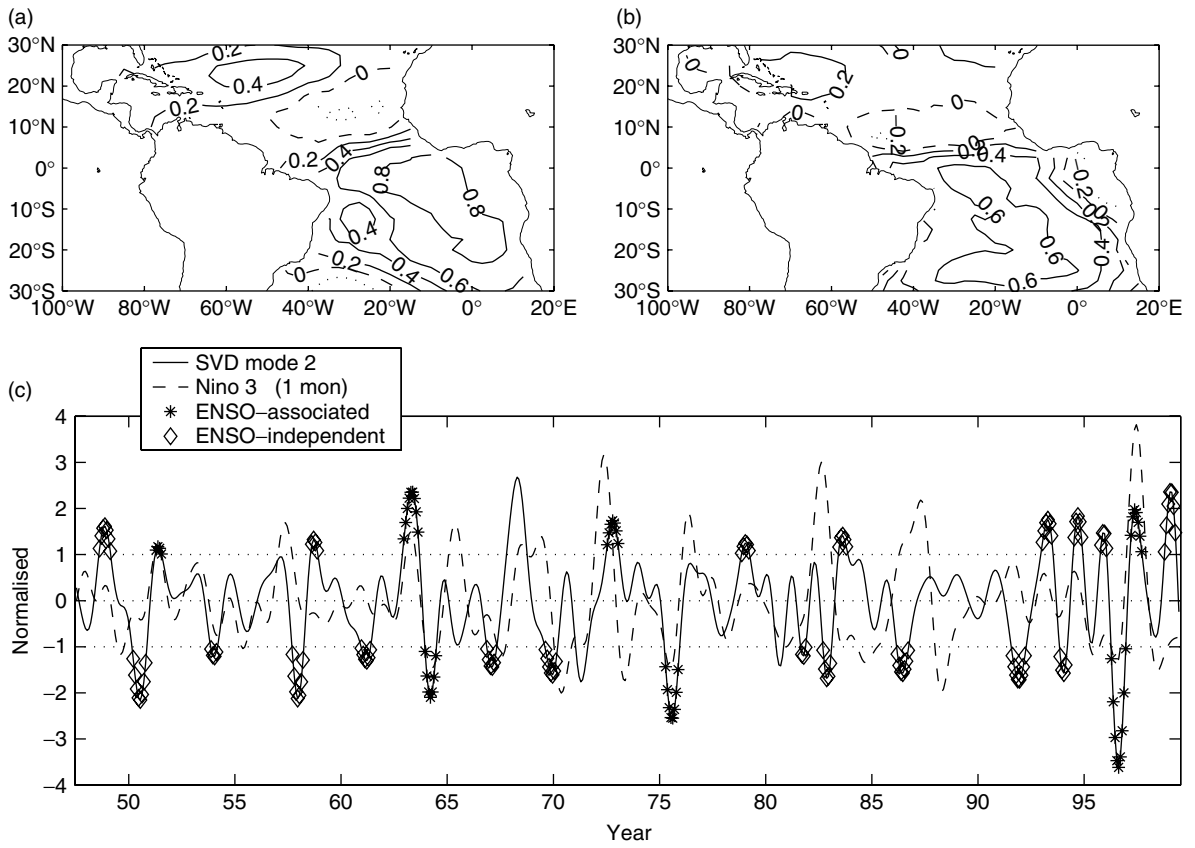

Figure 2. Anomaly correlation maps of SVD 2 over the Atlantic domain (30 °S–30 °N), (a) SST anomaly, (b) zonal wind stress anomaly. Contour interval is 0.2. Negative contours are dotted, and the zero contour is dashed. (c) Time series of A2 (solid line) and NINO3 lagged by 1 month (dashed line). Months included in the ENSO-associated and ENSO-independent composites are indicated by stars and diamonds, respectively

a positive correlation of similar magnitude ($r = 0.67$ for SVD1 and $r = 0.68$ for SVD2). Therefore, since the spatial structure of the SST anomalies shows a dynamical link to that of the τ_x anomalies, we define the arithmetic mean of the SVD SST and τ_x anomaly time series as the tropical Atlantic coupling indices: A1 and A2 for modes 1 and 2, respectively (Figures 1(c) and 2(c)).

We separated the variability in the tropical Atlantic occurring independently of ENSO from that occurring in conjunction with ENSO. Following Enfield and Mayer (1997), we calculated lag/lead correlations with standard ENSO indices. A1 has a maximum correlation with NINO 3.4 (averaged SST anomaly over 5 °S–5 °N, 170–120 °W) with a 4-month lag ($r = 0.59$); this is statistically significant at the 95% level. A2 has a maximum correlation with NINO3 (averaged SST anomaly over 5 °S–5 °N, 150–90 °W) with a 1-month lag ($r = 0.24$); this is only marginally significant. Of course, A2 shows a strong zero-lagged correlation with the equatorial Atlantic ATL3 index (averaged SST anomaly over 2.5 °S–2.5 °N, 20 °W–0 °E; $r = 0.85$). A2 also exhibits oscillations corresponding to past equatorial Atlantic warm–cold sequential events of 1949–1950, 1967–1971, 1983–1984, and 1996–1997. These types of events are generally not well correlated with El niño events, consistent with a purely internal mode of tropical Atlantic variability on interannual timescales (Handoh and Bigg, 2000; Tseng and Mechoso, 2001).

Composites for mode 1 of the tropical Atlantic variability were constructed by selecting months in which A1 > 1 (warm events) and those in which A1 < -1 (cold events). Those were then further subdivided into events that were classified to occur in conjunction with ENSO (ENSO-associated events), when the 4-month lagged NINO3.4 index was above 1 for the warm events and below -1 for the cold events. The remaining

Copyright © 2006 Royal Meteorological Society

DOI: 10.1002/joc

selected months were classified as ENSO-independent events with no associated ENSO signal. There were 7 (5) ENSO-associated warm (cold) NTA events and 7 (11) ENSO-independent warm (cold) NTA events (Figure 1(c)).

With the tropical Atlantic coupling indices (A1 and A2) we are able to examine any seasonal phase locking of NTA and STA events. Figure 3(a) shows the well-known seasonal phase locking of ENSO, with peaks over the boreal autumn–winter seasons in both warm (El Niño phase; NINO3.4 ≥ 1) and cold (La Niña phase; NINO3.4 ≤ -1) events. ENSO-associated NTA events peak in boreal spring (Figure 3(b)), reflecting the 4–5 month lagged response of the NTA to the Pacific ENSO (Enfield and Mayer, 1997; Saravanan and Chang, 2000; Mo and Häkkinen, 2001). In contrast, ENSO-independent warm events in the NTA occur mainly in autumn, whereas the corresponding cold events have no preferred season. This difference between warm and cold events has been previously reported for the equatorial Atlantic mode (Xie and Carton, 2004), but not for the NTA, partly because no rigorous distinction between ENSO-associated and ENSO-independent events was made in the previous studies.

The STA mode also displays a seasonal phase locking (Figure 3(c)). The ENSO-associated STA events show a similar seasonal phase lock to the Pacific ENSO (Figure 3(a)), with peaks over the boreal autumn–winter seasons. Interestingly, neither warm nor cold events occur during May to June. The seasonal phase locking of

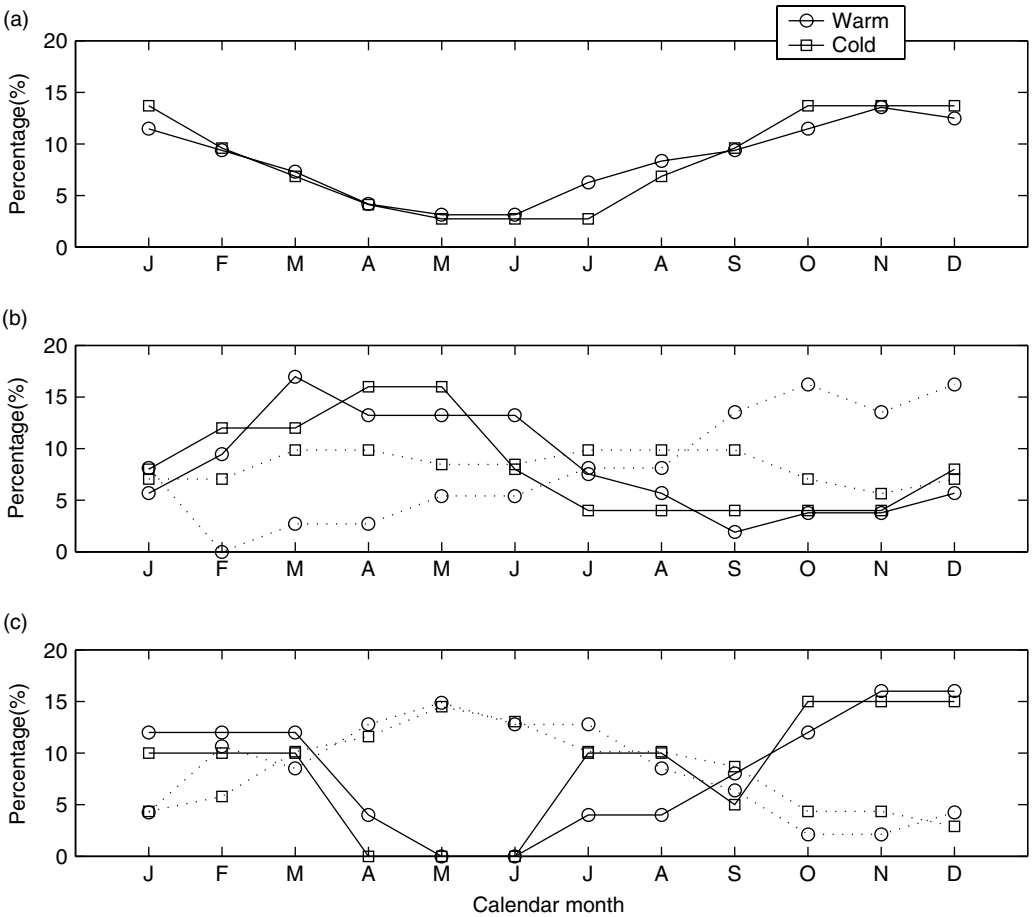

Figure 3. Seasonal phase locking of the climate events. Monthly distribution of the occurrence of warm (circle) and cold (square) events are given as a %. (a) ENSO characterised by NINO3.4, (b) North Tropical Atlantic (A1) mode and (c) South Tropical Atlantic (A2) mode. In (b) and (c), ENSO-associated and ENSO-independent events are denoted by solid and dotted lines, respectively

Copyright © 2006 Royal Meteorological Society

DOI: 10.1002/joc

the ENSO-independent STA events is out of phase with that of the ENSO-associated events. Neither ENSO-associated nor ENSO-independent STA events show the previously recognised boreal summer phase lock of the equatorial Atlantic (Xie and Carton, 2004).

In this paper we will henceforth focus on the NTA mode, while the STA mode will be discussed in a companion paper. Composite maps were constructed for warm and cold NTA events. Although the global response to ENSO signals is essentially non-linear (Pozo-Vazquez *et al*., 2001; Wu and Hsieh, 2004; Mariotti *et al*., 2005), our warm and cold event composites (both ENSO-associated and ENSO-independent events) had very similar patterns, but with the opposite sign, and are summarised here as an average of the warm minus cold pattern. This linearity occurs because in our composite method the primary criterion is the tropical Atlantic climate variability (A1), and the presence of ENSO is used as a secondary criterion.

A re-sampling technique was used to examine the statistical significance of the composite maps. Following Matthews and Kiladis (1999), 10 000 paired synthetic time series for A1 and the 4-month lagged NINO3.4 were created, with the same auto-correlation and cross-correlation characteristics as the original time series. The local significance of the composite patterns at each grid point was then tested at the 95% level against the distribution function calculated from the synthetic time series.

We have also constructed lag composites to examine the origin and evolution of warm and cold NTA events. For each warm (cold) NTA event, the month with a temporal maximum (minimum) of A1 was defined as month 0. Then, 3-month means centred over months −9, −6, −3, 0, 3, 6, and 9 were calculated to compute a series of lag/lead composite maps.

3. RESULTS AND DISCUSSION

3.1. Sea-surface temperature, wind stress and convection

Global SST and wind stress anomaly vectors for the NTA mode are shown for those events occurring in conjunction with ENSO (Figure 4(a)), and independent of ENSO (Figure 4(b)). In both cases, positive SST anomalies between 0.1–0.4 °C and southwesterly wind stress anomalies cover the northern tropical Atlantic, together with a band of weaker negative SST anomalies over the subtropical North Atlantic, comparable with the composite map of Mo and Häkkinen (2001). Outside the NTA region, the patterns are very different in the two cases.

For ENSO-associated events (Figure 4(a)), the largest SST anomalies are in the equatorial Pacific, as expected. There are no significant SST anomalies over the extratropical North Atlantic, but northeasterly wind stress anomalies extend into northern Europe from the central North Atlantic. The positive SST anomalies over the southern subtropical Atlantic can be identified as a response to El Niño events (Elliott *et al*., 2001; Liu *et al*., 2004). Over the equatorial strip, no statistically significant easterly wind stress anomalies appear, which reflects the weak correlation in Figure 1(b).

Other organised positive SST anomalies are found in the Indian Ocean and mid-latitude South Pacific, consistent with El Niño . Negative SST anomalies are clearly present in the North and South Pacific over the subtropical latitudes. These constitute a pan-Pacific quadrapole structure of SST anomalies similar to those found by Sutton *et al*. (2000) and Spencer and Slingo (2003).

In contrast to the ENSO-associated events, ENSO-independent NTA events show significant year-round SST anomalies only over the North Atlantic (Figure 4(b)). The SST anomalies in the North Atlantic exhibit a statistically significant tripole pattern, accompanied by consistent surface wind stress and implied latent heat flux anomalies. This tripole pattern based on the ENSO-independent NTA events is rather different from that derived from the NAO index (Ruiz-Barradas *et al*., 2000; Mo and Häkkinen, 2001; Peng *et al*., 2003), partly because of our 12- to 72-month bandpass filtered data. The former shows a 'horseshoe' pattern with positive SST anomalies over the entire Northern Hemisphere eastern Atlantic, while the latter is characterised by a distinct tripole that is most pronounced over DJF–MAM (Sutton *et al*., 2000), when wind anomalies attain their maxima. However, the spatial pattern of the ENSO-independent warm NTA events shown here is dominated by the period of September to December, due to the seasonal phase locking (Figure 4(b)) discussed in Section 2.3.

Copyright © 2006 Royal Meteorological Society

DOI: 10.1002/joc

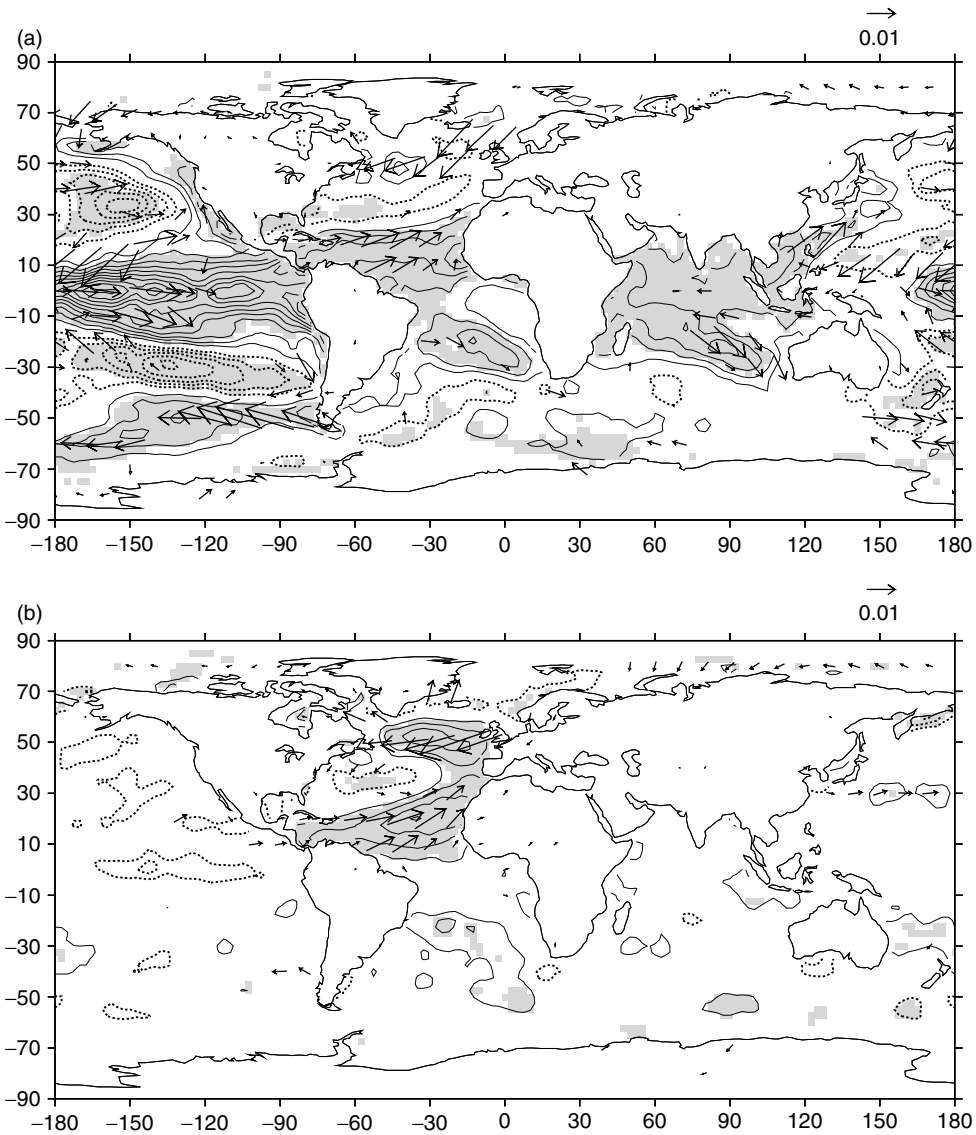

Figure 4. Global composite anomaly maps for the NTA mode (average of warm minus cold events) of SST anomalies and wind stress vectors, (a) ENSO-associated events, (b) ENSO-independent events. SST contour interval is 0.1 °C, and anomalies significant at the 95% level are shaded. Positive and negative anomalies are contoured by solid, and dotted lines, respectively. The zero contour is omitted. The reference surface wind stress vector is 0.01 Nm^{-2}, and vectors are only plotted (every 10 °) where either the x or y-component is significant

Composites of OLR were constructed using data from 1974 to 1999. There are seven ENSO-associated events (four warm and three cold) and eight ENSO-independent events (three warm and five cold). In contrast to SST, the OLR anomalies in the ENSO-associated and ENSO-independent events are very different over the NTA region (Figure 5). Consistent with the positive SST anomalies over the equatorial central and eastern Pacific for the ENSO-associated NTA event, deep convection was enhanced (negative OLR anomalies) in these regions and suppressed over Indonesia (Figure 5(a)). Over the tropical Atlantic sector, convection was suppressed (positive OLR anomalies) in the Intertropical Convergence Zone (ITCZ) along 10 °N, over the eastern equatorial Atlantic, and over the Amazon. Negative OLR anomalies over the Gulf of Mexico and the northern subtropical Atlantic indicate an enhancement of low-level stratocumulus associated with a decrease

Copyright © 2006 Royal Meteorological Society

DOI: 10.1002/joc

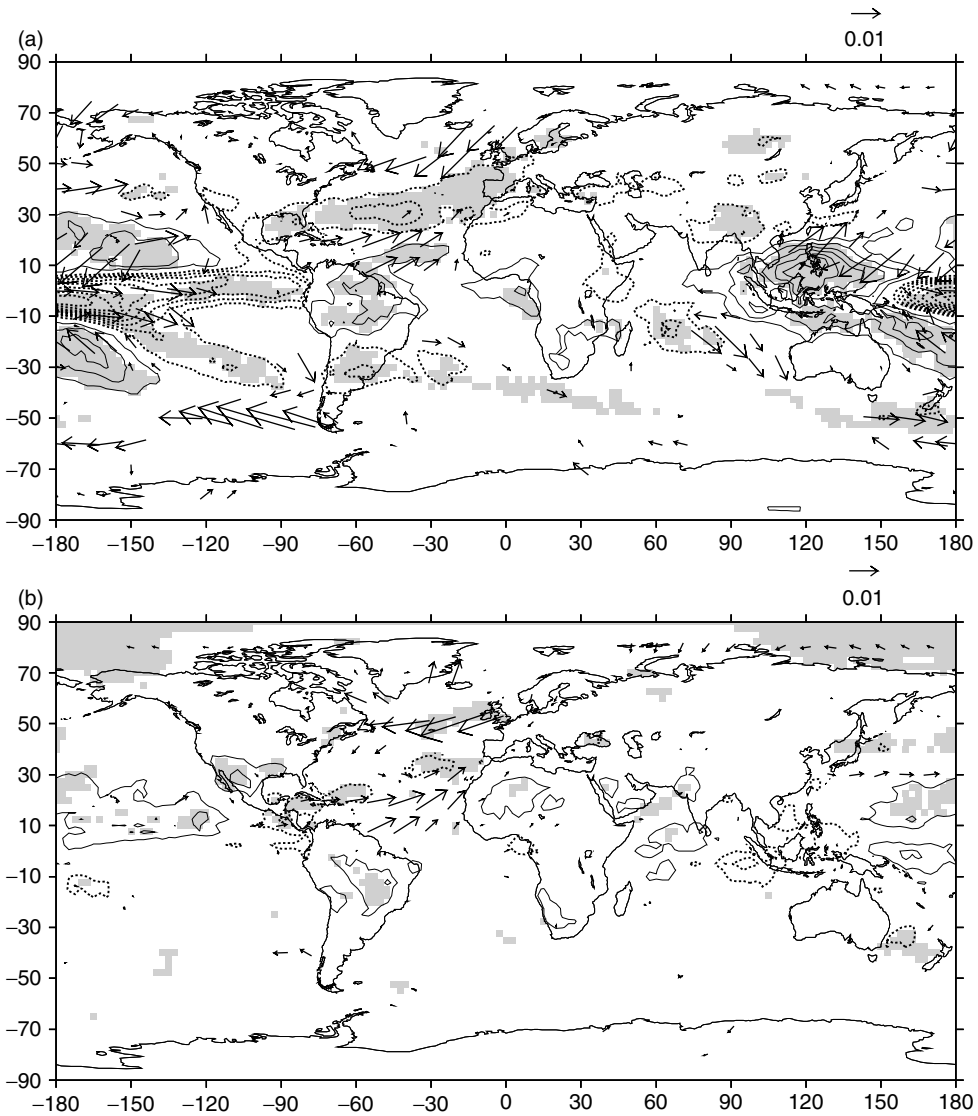

Figure 5. Same as Figure 4 but with OLR replacing the SST anomalies. Contour interval is 2.5 Wm^{-2} and significant anomalies are shaded. Positive and negative anomalies are contoured by solid, and dotted lines, respectively. The zero contour is omitted

in the strength of the Hadley Cell, confirmed by diagnosis of mid-latitude vertical velocity anomalies (not shown). This low-level cloud could contribute to the maintenance of negative SST anomalies that extended from Florida to southwestern Europe (Figure 4(a)) through a reduction in the surface shortwave radiation flux. This will be discussed further in Section 3.2. The overall distribution of OLR anomalies in the tropical Atlantic sector resembles that of cloud cover anomalies during ENSO (Klein *et al*., 1999). For ENSO-independent events, there are weak negative OLR anomalies over the western Caribbean (Figure 5(b)), associated with local positive SST anomalies, consistent with Giannini *et al*. (2001) hypothesis that rainfall anomalies in this region are due to a local thermodynamic response to SST anomalies.

3.2. Surface flux anomalies

Next we examine the surface heat fluxes associated with the events discussed in Section 3.1. Composites of these variables were constructed using data from 1983 to 1999. There are six ENSO-associated events

Copyright © 2006 Royal Meteorological Society

DOI: 10.1002/joc

(four warm and two cold) and six ENSO-independent events (three warm and three cold). Thus, the spatial structure of our heat flux anomalies in the North Atlantic may partially reflect the recent eastward shift of interannual NAO variability and shift to a higher NAO index (Jung *et al*., 2003).

During ENSO-associated events (Figure 6(a)), positive latent heat flux anomalies (oceanic gain of heat) of up to 16 Wm^{-2} cover the northern tropical Atlantic where SST anomalies are positive (Figure 4(a)). These anomalies are associated with a reduction in the strength of northeasterly trade winds. A weak negative latent heat flux anomaly over the subtropical North Atlantic is consistent with the regional negative SST anomaly. Another organised latent heat flux anomaly is found south of Iceland and east of Newfoundland in the North Atlantic, but is not associated with an SST anomaly (Figure 4(a)).

Both the incident surface shortwave and surface longwave radiation flux anomalies are significantly smaller than those of latent heat flux. To some degree, the pattern of incident shortwave radiation anomalies is very similar to that for OLR (Figure 5(a)) because enhanced (suppressed) convection and cloudiness reduces (increases) solar insolation. Shortwave radiation anomalies tend to damp the SST anomalies, but their forcing is partially cancelled out by longwave radiation anomalies. For example, increased cloudiness reduces the surface shortwave radiation by reflecting it back to space and increasing the incident surface longwave radiation by an increased greenhouse effect. The total heat flux anomalies at the sea-surface are dominated by latent heat flux anomalies (Figure 6(c)). Thus, the latent heat flux tends to maintain the SST anomalies in the northern tropical Atlantic. Negative total flux anomalies across the central Atlantic from western Europe (Figure 6(c)) are due to the low-level stratocumulus identified in Figure 5(a).

For the ENSO-independent events in the NTA, organised latent heat flux anomalies are restricted to the Atlantic basin (Figure 6(b)), as was found with the SST anomalies. Once again, the overall pattern of SST and heat flux anomalies in the north tropical Atlantic is mainly determined by the latent heat flux anomalies.

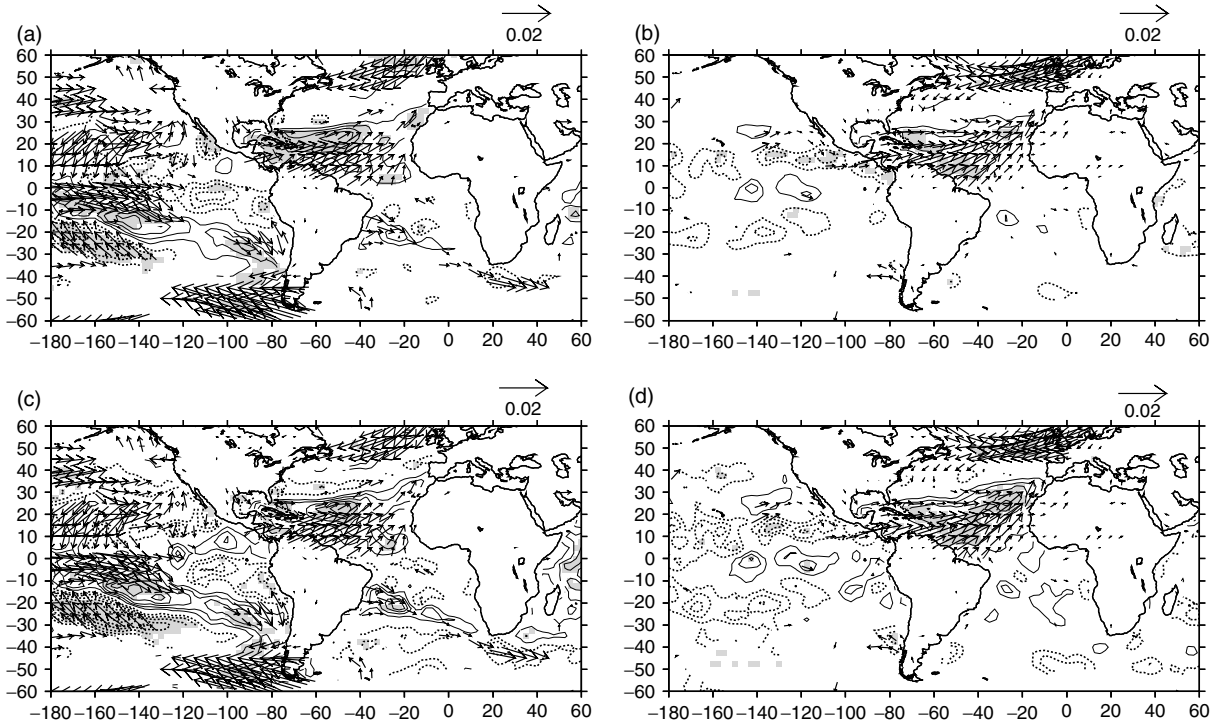

Figure 6. Composite anomaly maps (SVD 1) of latent heat flux and surface wind stress vectors for (a) ENSO-associated NTA events, (b) ENSO-independent NTA events, and of total surface flux and surface wind stress vectors (c) ENSO-associated NTA events and (d) ENSO-independent NTA events. Contour interval is 4 Wm^{-2} and significant anomalies are shaded. Positive and negative anomalies are contoured by solid, and dotted lines, respectively. The zero contour is omitted. Reference wind stress vector is 0.02 Nm^{-1} and vectors are only plotted (every 5°) where either the x or y-component is significant

Copyright © 2006 Royal Meteorological Society

DOI: 10.1002/joc

Now we consider the apparent ocean–atmosphere interactions identified above. Positive SST anomalies over the North Tropical Atlantic are associated with negative SLP anomalies and anomalous lower tropospheric cyclonic circulation over the subtropical latitudes (Figure 7). This can be attributed to the weakening of the Hadley Circulation (suppressed ascending air over the equatorial region and descending air over the sub-tropics), consistent with the distribution of vertical velocity anomalies (not shown). The associated wind anomalies weaken the prevailing background easterly trade winds, which in turn reduces surface evaporation and hence produces the observed latent heat flux anomaly, maintaining a positive SST anomaly.

This appears to be an oceanic response to atmospheric wind anomalies. There is no evidence of the ocean driving the atmospheric anomaly, hence the WES feedback loop is not closed. The WES feedback usually involves cross-equatorial surface wind anomalies due to a displacement or weakening of the ITCZ that is not seen at all in the ENSO-independent case but only in the ENSO-associated case in boreal summer (not shown). Such equatorial wind anomalies are pronounced in the decadal timescale Atlantic dipole or meridional mode structure (Okumura *et al*., 2001); they maximise the meridional gradient of SST anomalies. However, SST anomalies over either the North Tropical Atlantic or South Tropical Atlantic alone can provide a significant SST gradient and maintain the feedback system (Okumura *et al*., 2001), so the dipole structure is not essential to the WES mechanism.

Our analysis is consistent with previous studies (Czaja *et al*., 2002; Joyce *et al*., 2004) that identified ocean–atmosphere interaction over the NTA as not being part of the positive WES feedback loop. We will explore the conditions under which a WES feedback could work in Section 4.

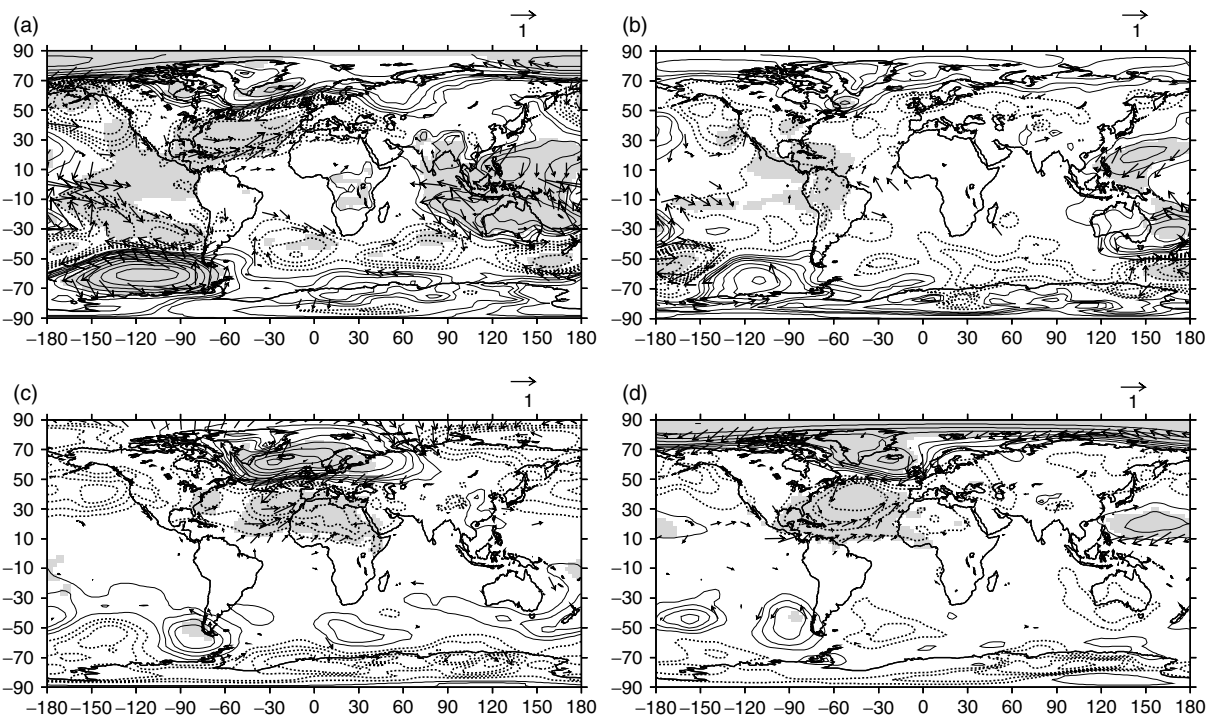

Figure 7. Global composite anomaly maps (SVD 1) for SLP and 1000 hPa vector wind anomalies. Contour interval is 0.25 hPa between −1 hPa and 1 hPa, and otherwise is 0.5 hPa. Significant anomalies are shaded. ENSO-associated events for (a) DJF, (b) JJA. ENSO-independent events for (c) DJF, (d) JJA. Positive and negative anomalies are contoured by solid, and dotted lines, respectively. The zero contour is omitted. Reference wind vector is 1 ms^{-1} and vectors are only plotted (every 10°) where either the x or y-component is significant

Copyright © 2006 Royal Meteorological Society

DOI: 10.1002/joc

3.3. Lower and upper tropospheric anomalies

In this section, we describe the global significance of the NTA mode during boreal winter (DJF) and summer (JJA) for the sea-level pressure, and streamfunction and wind vectors on the 200 hPa surface. For the ENSO-associated NTA events, distinct negative SLP anomalies are located in the subtropical to middle latitudes in the North Atlantic during DJF (Figure 7(a)), consistent with reports of Mo and Häkkinen (2001). Together with a significant positive SLP anomaly over Iceland, this forms a SLP dipole pattern similar to the NAO. Over the tropical Pacific, 1000 hPa westerly anomalies are indicative of the El Niño conditions. In the upper troposphere (Figure 8(a)), the twin tropical anticyclonic anomalies over the Pacific can be interpreted as the equatorial Rossby wave response to the anomalous heating over the Pacific. There is an associated extratropical wave train that projects strongly onto the PNA pattern, with a cyclonic anomaly over the central North Pacific, an anticyclonic anomaly over Canada, and a cyclonic anomaly over the eastern United States. This latter cyclonic anomaly extends down to the surface and is manifested in the low-pressure anomaly over the western subtropical Atlantic (Figure 7(a)). Hence, the surface southwesterly wind anomalies over the subtropical Atlantic, which are responsible for the reduction in evaporation and warm SSTs in this region, can be attributed partially to an extratropical wave train forcing from El Niño.

In the Southern Hemisphere, a PSA teleconnection pattern (Mo and Paegle, 2001) is present, linking Australia to the South Atlantic via the Southern Ocean. The PSA pattern is evident in both the lower (Figure 7(a)) and upper troposphere (Figure 8(a)). These remote forcings appear to induce the westerly wind anomalies over the southern subtropical Atlantic, which lead to the positive SST anomalies through a reduction in the latent heat flux (Figure 4(a)). During northern summer, the ENSO-associated NTA events are weak (Figures 7(b) and 8(b)) with little significant signal over the Atlantic region.

During ENSO-independent NTA events, significant atmospheric features are largely restricted to the Atlantic and adjacent continents in the Northern Hemisphere (Figures 7(c), 7(d), 8(c), and 8(d)); no wave trains appear in the Southern Hemisphere. Over the northern tropical to subtropical Atlantic, negative SLP anomalies of

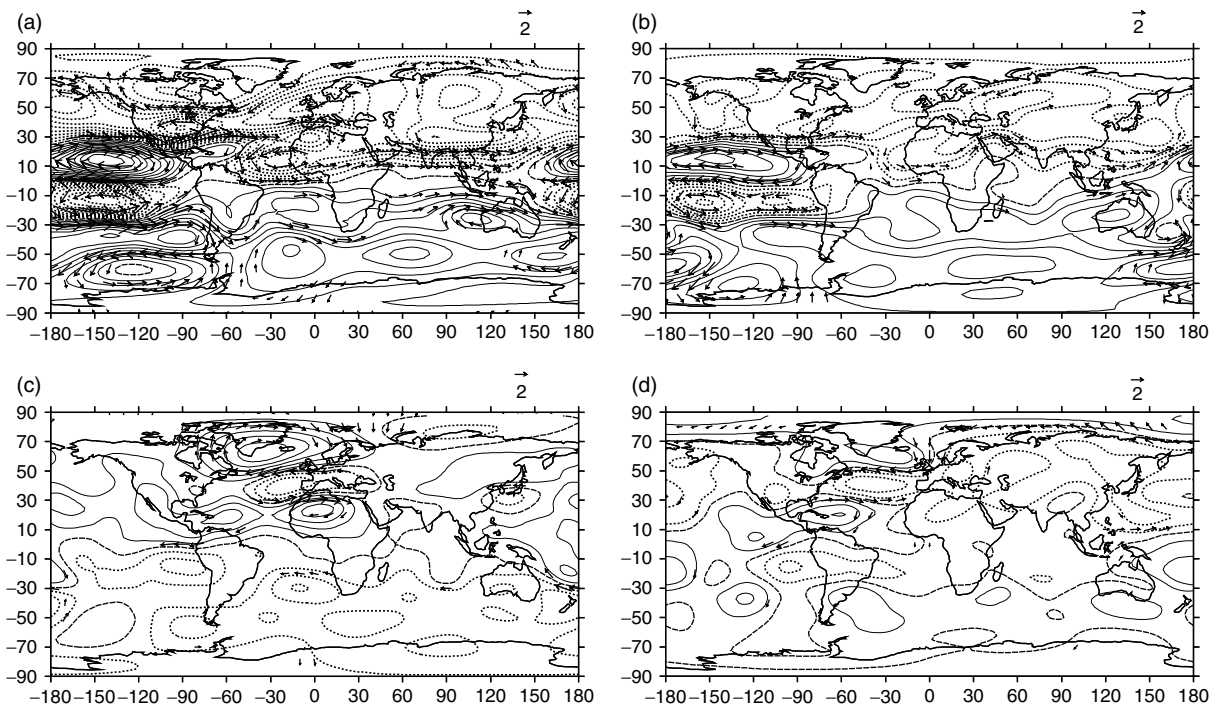

Figure 8. Same as Figure 7 but for the 200 hPa level stream function and vector wind anomalies. Stream function contour interval is 8×10^5 $m^2 s^{-1}$. Positive and negative anomalies are contoured by solid and dotted lines, respectively. The zero contour is dashed. Reference wind vector is 2 ms^{-1} and vectors are only plotted (every 10°) where either the x- or y-component is significant

Copyright © 2006 Royal Meteorological Society

DOI: 10.1002/joc

up to −1.0 hPa are present (Figure 7(c) and (d)), with an associated cyclonic circulation anomaly. Positive SLP anomalies are located further north over the eastern mid-latitude Atlantic, leading to corresponding northeasterly wind anomalies over the North Atlantic. The positive SLP anomaly shifts eastward from summer to winter (Figure 7(c) and (d)). The anticyclonic anomaly over the northern mid-latitude Atlantic weakens during the boreal summer (Figure 7(d)). At the 200 hPa level, a similar barotropic anomaly is found (Figure 8(c)), providing strong easterly wind anomalies over Britain during winter. These characteristics at both the surface and upper tropospheric levels are very similar to those of a typical NAO pattern, associated with SST tripole anomalies (Sutton *et al*. 2001). Over the North Tropical Atlantic, there is an anticyclonic anomaly, with two peaks over the west Caribbean (consistent with the negative OLR anomalies and enhanced convection in Figure 5(b)) and northwest Africa in winter (Figure 8(c)).

The upper tropospheric anomaly patterns in the ENSO-independent NTA events differ between the seasons. During winter (Figure 8(c)), the extratropical anticyclonic anomaly that forms part of the NAO pattern is strong, indicating that extratropical forcing of the NTA is important (Czaja *et al*., 2002). However, during summer this anticyclonic anomaly is much reduced, and the pattern is consistent with an extratropical response to the enhanced heating over the Caribbean (Ferranti *et al*., 1994).

3.4. Dynamic evolution of the anomalies

Here we examine the time evolution of the anomaly patterns, using lagged composite maps of anomalous SST and surface wind vectors (Figure 9) and upper and lower tropospheric circulation (Figures 10 and 11). See Section 2.3 for a description of how the lags are defined.

3.4.1. ENSO-associated NTA event. The evolutions of anomalies during an ENSO-associated NTA event are similar to those described in Saravanan and Chang (2000) and Mo and Häkkinen (2001). Negative SST anomalies over the 35°–60 °N band are identified in the North Atlantic in month −6 (Figure 9(a)). These are consistent with enhanced evaporation caused by a weak strengthening of the westerlies over the southern edge of a barotropic cyclonic anomaly extending from the surface to 200 hPa (Figure 10(b) and (g)). This anomaly is part of the PNA-like wave train emanating from the central Pacific (month −9; Figure 10(f)), consistent with the atmospheric response to El Niño (Spencer and Slingo, 2003). By month −3, the 200 hPa equatorial Rossby wave response to the Pacific SST anomalies has moved eastward to the eastern Pacific (Figure 10(h)). The extratropical response changes with it, such that the cyclonic anomaly over the North Atlantic moves further south, and its northern edge leads to weaker westerlies (Figure 10(c) and (d)) and a transition to positive SST anomalies over the far North Atlantic by month 0 (Figure 9(c) and (d)).

In the sub-tropics, by month −3 the southern edge of the cyclonic anomaly (Figures 9(b), 10(c), and (h)) leads to the weakening of the easterly trades and causes SST to rise by reducing evaporation (Figure 9(b) and (c)). A narrow zonal band of negative SST anomalies over the sub-tropics is also developed, probably due to the enhanced westerlies and increased evaporative cooling or the cooling effect from anomalous amounts of low-level stratocumulus formed (Figure 5(a)) in response to the reduced surface wind divergence from the subtropical high.

The equatorial Rossby wave response (upper tropospheric anticyclonic anomalies) to anomalous heating (Figure 10(g)) over the tropical Pacific does not directly influence the tropical Atlantic, but there are strong upper tropospheric westerly anomalies over the equatorial Atlantic, which can be attributed to an equatorial Kelvin wave response. Weak near-surface equatorial easterly anomalies over the western equatorial Atlantic are also identified (Figure 10(b)), indicative of an anomalous Walker circulation.

3.4.2. ENSO-independent NTA event. In contrast to the ENSO-associated NTA events, there are no strong anomalous tropospheric wind vectors in month −9 of the ENSO-independent NTA event (Figure 11(a) and (f)). By month −6, southwesterly surface wind anomalies have developed over the North Atlantic (Figure 9(f)) as part of a large-scale cyclonic anomaly. This has an approximately equivalent barotropic structure in the vertical and extends upward into the troposphere (Figure 11(b) and (g)), where it forms part of a wave train originating from near 100 °W in the Pacific–North America region, but its orientation and

Copyright © 2006 Royal Meteorological Society

DOI: 10.1002/joc

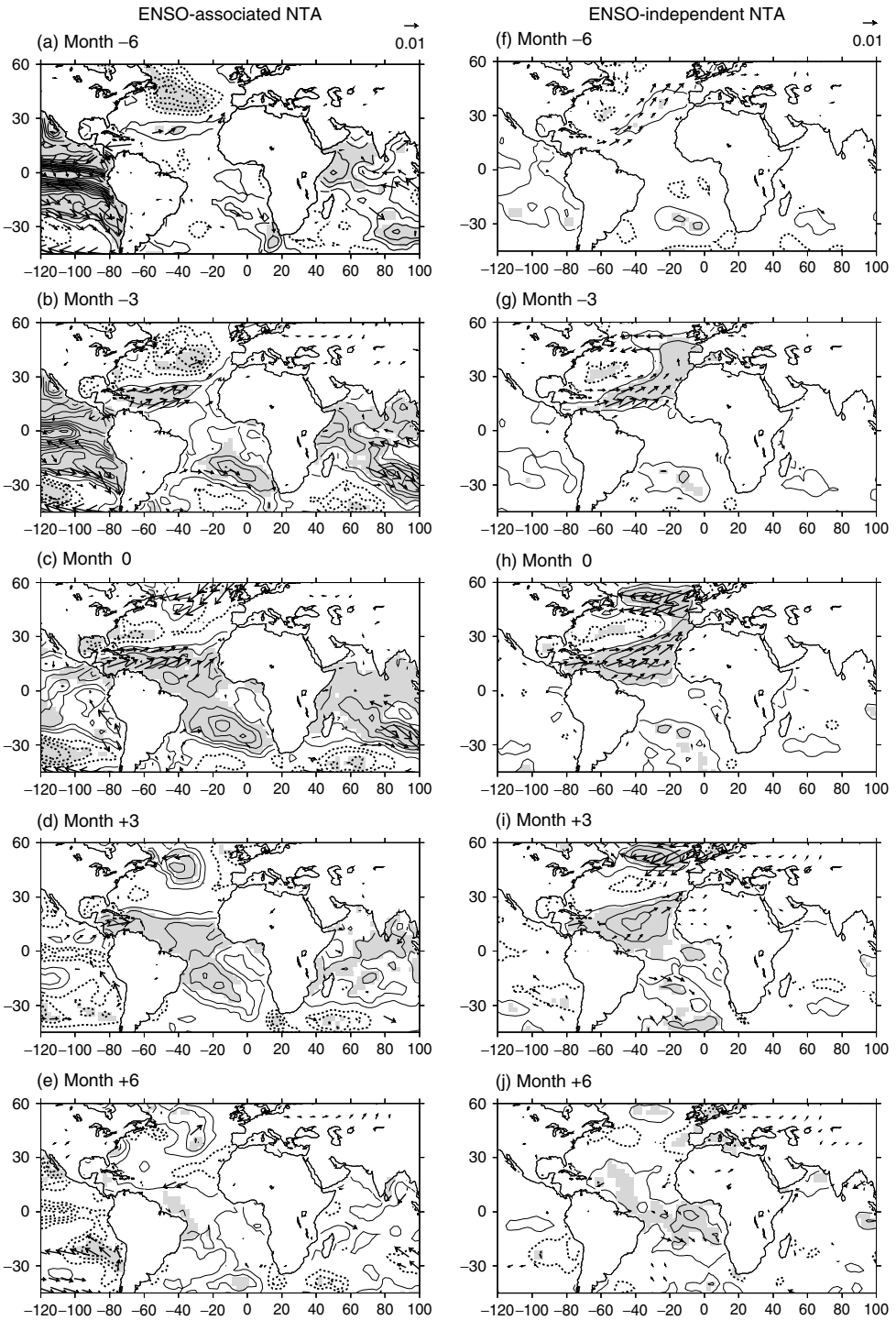

Figure 9. Lag composite maps for SST and surface wind vectors anomalies. (a) −6, (b) −3, (c) 0, (d) +3, and (e) +6 months for ENSO-associated NTA events. (f) −6, (g) −3, (h) 0, (i) +3, and (j) +6 months for ENSO-independent NTA events. For each warm (cold) NTA event, the month with a temporal maximum (minimum) of A1 was defined as month 0. SST anomaly contour interval is 0.1 °C, and significant anomalies are shaded. Positive and negative anomalies are contoured by solid and dotted lines, respectively. The zero contour is omitted. The reference surface wind stress vector is 0.01 Nm^{-2}, and vectors are only plotted (every 7.5°) where either the x or y-component is significant

Copyright © 2006 Royal Meteorological Society

DOI: 10.1002/joc

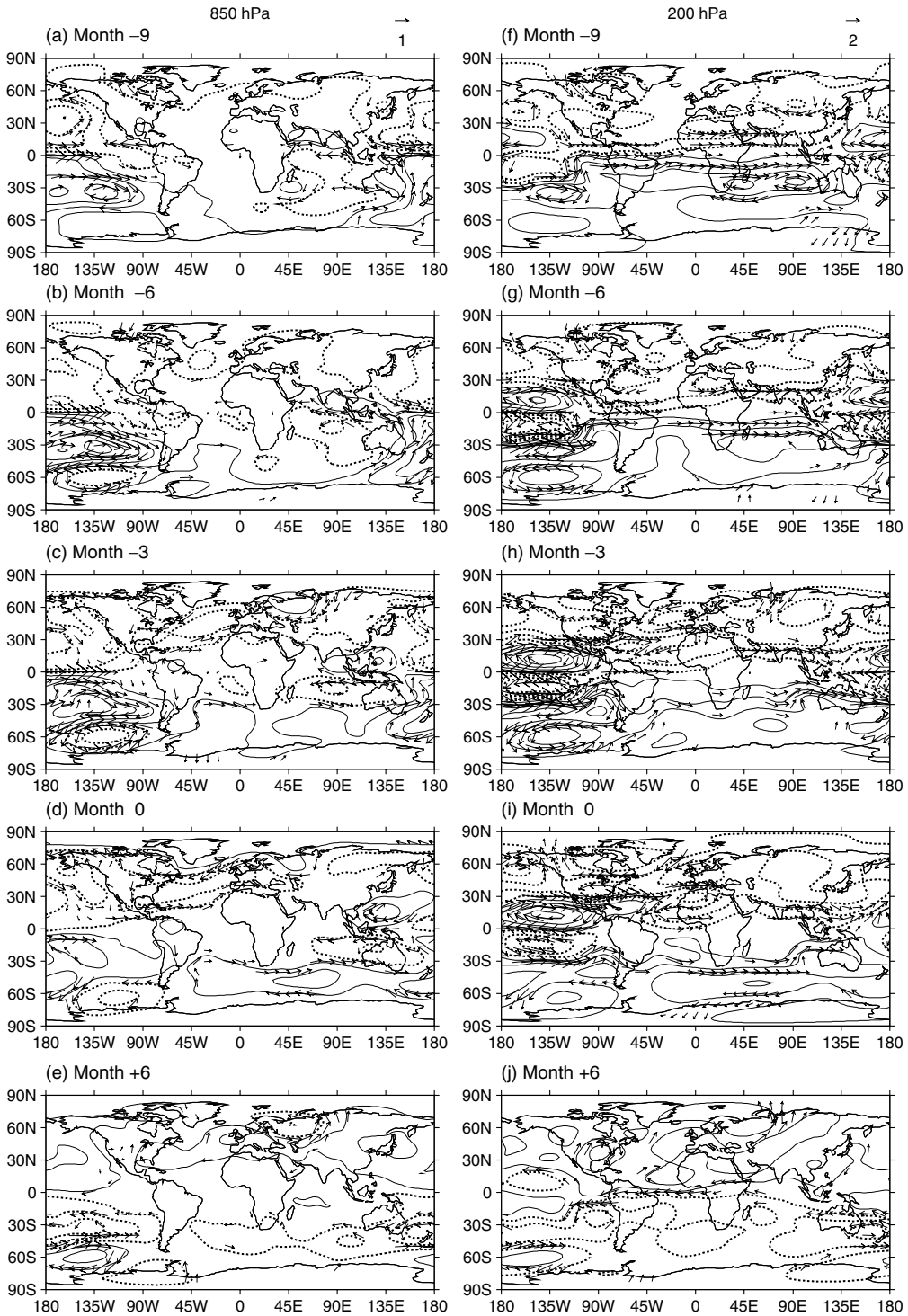

Figure 10. Lag composite maps for 850 and 200 hPa stream function, and vector wind anomalies for ENSO-associated NTA events. (a, f) −9, (b, g) −6, (c, h) 3, (d, i) 0, and (e, j) +6 months for 850 and 200 hPa level, respectively. Stream function contour intervals are 6 and 12×10^5 m^2 s^{-1} for 850 and 200 hPa levels, respectively. Positive and negative anomalies are contoured by solid and dotted lines, respectively. The zero contour is omitted. Reference wind vectors are shown on the top of (a) and (f). Vectors are only plotted (every 7.5°) where either the x or y-component is significant

Copyright © 2006 Royal Meteorological Society

DOI: 10.1002/joc

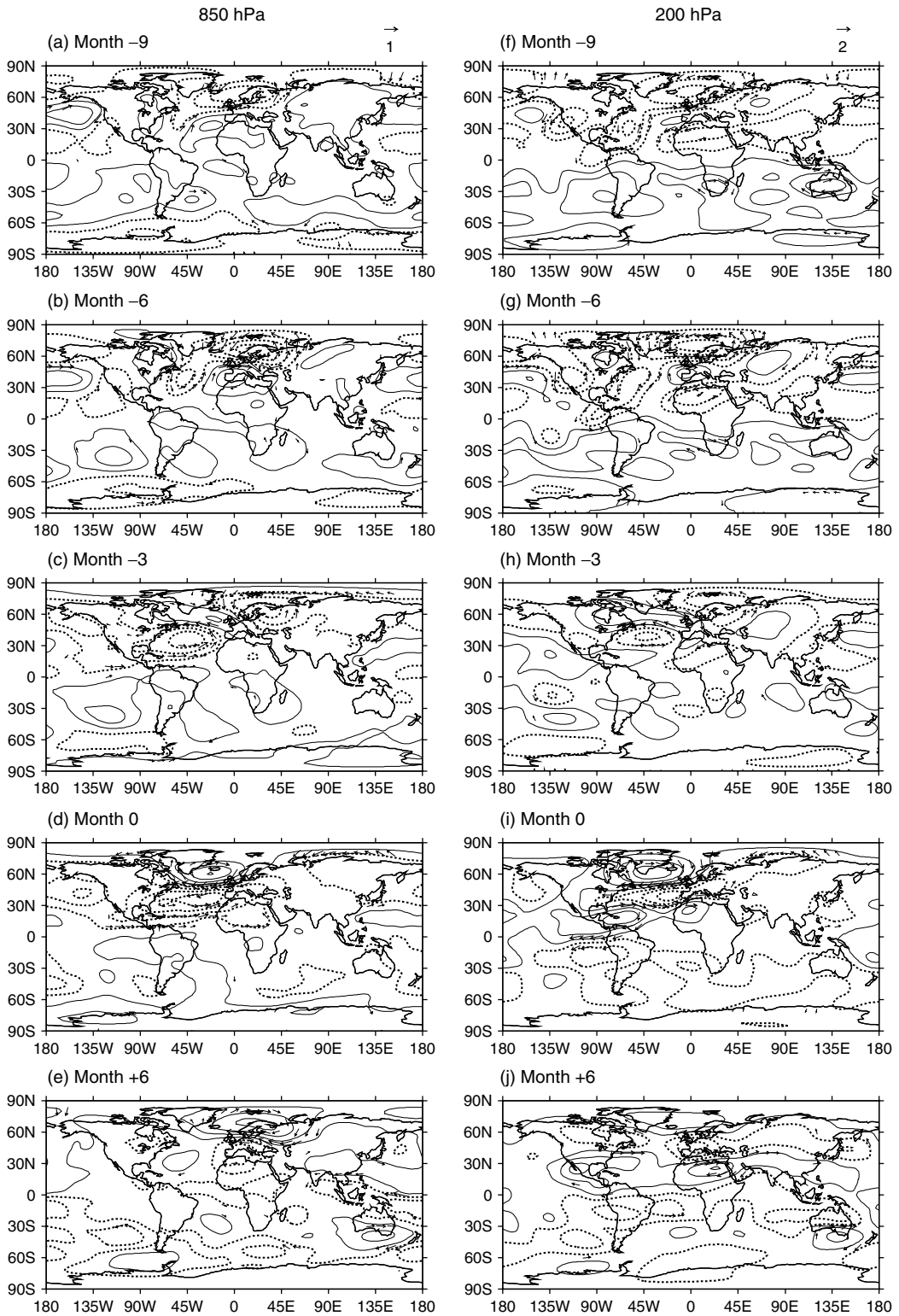

Figure 11. Same as Figure 10, but for ENSO-independent events. Stream function contour intervals are 4 and 8×10^5 m^2 s^{-1} for 850 and 200 hPa levels, respectively

Copyright © 2006 Royal Meteorological Society

DOI: 10.1002/joc

magnitude is different and less robust to that in the ENSO-associated case. This wave train appears to split into a high zonal wave number component that is deflected equatorward (Hoskins and Karoly, 1981), and a low zonal wave number component that propagates towards the higher latitudes over northern Europe and Eurasia. This barotropic Rossby wave propagation could be guided by the North Atlantic jet (Hoskins and Ambrizzi, 1993).

The cyclonic gyre over the North Atlantic then develops a more zonal orientation over subtropical to middle latitudes in month −3 (Figures 9(g), 11(c) and (h)). The resulting weakening of the northeasterly trades in the tropics and the westerlies in mid-latitudes suppresses surface evaporation and causes SST to rise. These positive SST anomalies are extended to the west of western Europe. This leads to a distinct horseshoe pattern of SST anomalies in month 0 (Figure 9(h)), and wind anomalies are enhanced. At this stage (months −3 and 0), a distinct NAO pattern develops through the depth of troposphere (Figures 9(c), 11(c) and (d)), which is similar to that in the winter season (Figure 8(c)). We speculate that part of this could be attributed to a Rossby wave train that is excited in the western Caribbean, west of the SST anomalies in the NTA (Figure 11(c) and (d)); the upper tropospheric anomalies in the tropics resemble Saravanan and Chang's (2000) atmospheric GCM response to the NTA SST anomalies. The lower tropospheric cyclonic equatorial Rossby wave response to the positive SST anomalies might play an important role over months −3 to 3 (Figure 9(g)–(i)) in weakening the easterly trades over the NTA. The SST anomalies (Figure 9(i)) weaken in the tropics in month 3. Both surface and tropospheric anomalies in the North Atlantic have disappeared by month +6 (Figures 9(j) and 11(e)).

Hence, ENSO-independent NTA events seem to be induced by an extratropical wave train originating from the Pacific. We speculate that the NTA events could be triggered by stochastic forcing in the Pacific as we are here considering the periods when ENSO signals are not significant.

4. CONCLUSIONS

We have examined the interannual ocean–atmosphere variability of the tropical Atlantic employing the 12- to 72-month bandpass filtered data sets. Using SVD analysis of SST and zonal wind stress anomalies, we have constructed global composite maps of various climate variables associated with the NTA ocean–atmosphere mode. In a companion paper (Handoh *et al*., 2006) we examine the STA modes.

There is a clear difference between the NTA events that occur with ENSO and those that occur independently of ENSO. For the ENSO-associated events, SST and zonal wind stress anomalies in the North Tropical Atlantic lag ENSO by 4 months. This is consistent with Enfield and Mayer's (1997) second EOF mode of SST anomalies, and Mo and Häkkinen's (2001) lag composite analysis. Our analysis suggests that the ENSO-associated events seem to be forced by an extratropical PNA-like wave train emanating from the Pacific rather than a change in the Walker circulation due to the equatorial Kelvin wave response to ENSO. This is consistent with Nobre and Shukla (1996) and Sutton *et al*. (2000) who found that off-equatorial tropical Atlantic events are unlikely to be induced by a change in Walker circulation.

The ENSO-independent case showed that the tropical Atlantic anomalies could also be forced by an extratropical pattern that originated over the Pacific. This suggests that NTA events could be induced by non-ENSO stochastic forcing. Subsequent development of anomalies over the Atlantic sector were then consistent with the atmospheric response to NTA SST anomalies. Our results suggest that in both ENSO-associated and ENSO-independent cases for the NTA mode, SST and surface wind stress variability on interannual timescales are induced by external forcing. In the ENSO-independent NTA events the induced anomalies can be maintained by local ocean–atmosphere interaction (Liu *et al*., 2004).

Ocean–atmosphere coupling processes were examined. The WES feedback (Xie and Philander, 1994) is not a plausible mechanism that help in maintaining the mode over the North Tropical Atlantic during the ENSO-independent events. The magnitude of SST anomalies (0.1–0.4 °C) may not be large enough to displace the ITCZ towards the warmer hemisphere. It appears to be the atmospheric wind anomaly driving an SST anomaly through thermodynamic interaction, rather than a full coupling. This is significantly different from the case for the tropical dipole structure on decadal timescales (Peng *et al*., 2000; Okumura *et al*., 2001), in which

Copyright © 2006 Royal Meteorological Society

DOI: 10.1002/joc

the magnitude of SST anomalies is more than twice as large as in the interannual timescale ENSO-associated and ENSO-independent events. In addition, with both ENSO-associated and ENSO-independent cases there are no significant cross-equatorial flows that lie at the heart of the tropical WES feedback mechanism.

A possible key mechanism to establish a two-way ocean–atmosphere WES feedback (without the presence of cross-equatorial wind anomalies) is a Rossby wave response to the SST anomalies north of the equator. During ENSO-independent events, significant cyclonic anomalies appear in the North Atlantic (Section 3.2). They exhibit a baroclinic structure through the depth of the atmosphere over the NTA (Figures 7(d) and 8(d)). This can be interpreted as the off-equatorial Rossby wave response to the diabatic heating associated with the NTA SST anomalies (Ruiz-Barradas *et al*., 2000) in the NTA. The southwesterly anomalies on the equatorward side of the Rossby cyclonic anomaly cause the SST to rise through suppression of evaporation, which then reinforces the equatorial Rossby wave. Hence, the positive WES feedback loop is closed, without the presence of cross-equatorial winds or an SST dipole, provided the damping rate of SST anomalies is smaller than the growth rate of the ocean–atmosphere coupling (Czaja *et al*., 2002). However, a recent study suggests that only a weak positive feedback is at work over the deep tropics of 10 °S–10 °N (Joyce *et al*., 2004).

Our composite analysis has revealed that the ENSO-independent events have enhanced convection over the tropical Atlantic and excite a wave train from the tropical Atlantic to mid- to high-latitudes in Northern Hemisphere, while the ENSO-associated events do not, as the external forcing from ENSO acts to suppress convection over the tropical Atlantic. We suggest that the diabatic heating associated with convective activity in the west Caribbean (Ruiz-Barradas *et al*., 2003) during the ENSO-independent NTA event is responsible for the excitement of the wave train.

In future work, composite maps of the SST anomalies for the ENSO-associated and ENSO-independent cases will be used to force an atmospheric GCM in order to examine the details of the ocean–atmosphere interaction for each case. According to Czaja *et al*. (2002), the NAO tripole pattern can be maintained by a positive dynamic feedback between the ocean and the atmosphere–the SST tripole induces the NAO anomalous atmospheric circulation (Sutton *et al*., 2001), and *vice versa* (Marshall *et al*., 2001). Thus, there appears to be some evidence of two-way ocean–atmosphere feedback processes in the North Tropical Atlantic. However, the magnitude of SST anomalies used as forcing in previous modelling studies, such as by Okumura *et al*. (2001), may be too large to be compatible with the results of observational evidence. In fact, a distinct interannual dipole structure of the tropical Atlantic is not found in our analysis, while it is seen in their model forcing. The atmospheric response to SST anomalies in the NTA may depend in a non-linear way on the magnitude of the anomalies.

ACKNOWLEDGEMENTS

The NCEP-NCAR re-analysis and OLR data were obtained from the Climate Diagnostics Center (http://www.cdc.noaa.gov). SST data were provided by the British Atmospheric Data Centre. Satellite-derived data to estimate shortwave and longwave radiations were provided by the International Satellite Cloud Climatology Project (ISCCP; http://isccp.giss.nasa.gov). We thank the two anonymous reviewers and COAPEC colleagues for constructive criticisms and useful discussions, respectively, which helped us to improve the manuscript. ICH has been financially supported by the NERC COAPEC programme (NER/T/S/2000/00295).

REFERENCES

Bishop JKB, Rossow WB. 1991. Spatial and temporal variability of global surface solar irradiance. *Journal of Geophysical Research* **96**: 16839–16858.

Bretherton CS, Smith C, Wallace MJ. 1992. An intercomparison of methods for finding coupled patterns in climate data. *Journal of Climate* **5**: 541–560.

Carton JA, Huang B. 1994. Warm events in the tropical Atlantic. *Journal of Physical Oceanography* **24**: 888–903.

Carton JA, Cao X, Giese BS, da Silva AM. 1996. Decadal and interannual SST variability in the tropical Atlantic Ocean. *Journal of Physical Oceanography* **26**: 1165–1175.

Chang P, Ji L, Li H. 1997. A decadal climate variation in the tropical Atlantic Ocean from thermodynamic air–sea interactions. *Nature* **385**: 516–518.

Chang P, Saravanan R, Ji L. 2003. Tropical Atlantic seasonal predictability: the roles of El niño remote influence and thermodynamic air–sea feedback. *Geophysical Research Letters* **30**: 1501, DOI: 10.10029/2002GL016119.

Copyright © 2006 Royal Meteorological Society

Chang P, Saravanan R, Ji L, Hegerl GC. 2000. The effect of local sea surface temperature on atmospheric circulation over the tropical Atlantic sector. *Journal of Climate* **13**: 2195–2216.
Curtis S, Adler R, Huffman G, Nelkin E, Dolvin D. 2001. Evolution of tropical and extra-tropical precipitation anomalies during the 1997–1999 ENSO cycle. *International Journal of Climatology* **21**: 961–973.
Czaja A, van der Vaart P, Marshall J. 2002. A diagnostic study of the role of remote forcing in tropical Atlantic variability. *Journal of Climate* **15**: 3280–3290.
Darnell WL, Gupta SK, Staylor WF. 1983. Downward longwave radiation at the surface from satellite measurements. *Journal of Climate and Applied Meteorology* **22**: 1956–1960.
Delecluse P, Servain J, Levy C, Arpe K, Bengtsson L. 1994. On the teleconnection between the 1984 Atlantic warm event and the 1982-83 ENSO. *Tellus* **46**: 448–464.
Dommenget D, Latif M. 2000. Interannual to decadal variability in the tropical Atlantic. *Journal of Climate* **13**: 777–792.
Elliott J, Jewson SP, Sutton RT. 2001. The impact of the 1997/98 El Niño events on the Atlantic Ocean. *Journal of Climate* **14**: 1069–1077.
Enfield DB, Mayer DA. 1997. Tropical Atlantic sea surface temperature variability and its relation to El Niño-Southern Oscillation. *Journal of Geophysical Research* **102**: 929–945.
Fairall CW, Bradley EF, Rogers DP, Edson JB, Young GS. 1996. Bulk parameterization of air–sea fluxes for tropical ocean-global atmosphere coupled-ocean atmosphere response experiment. *Journal of Geophysical Research* **101**: 3474–3764.
Ferranti L, Molteni F, Palmer TN. 1994. Impact of localised tropical and extratropical SST anomalies in ensembles of seasonal GCM integrations. *Quarterly Journal of the Royal Meteorological Society* **120**: 1613–1645.
Giannini A, Chiang JCH, Cane MA, Kushnir Y, Seager R. 2001. The ENSO teleconnection to the tropical Atlantic Ocean: contributions of the remote and local SSTs to rainfall variability in the tropical Americas. *Journal of Climate* **14**: 4530–4544.
Gupta SK, Darnell WL, Wilber AC. 1992. A parameterization for longwave surface radiation from satellite data: Recent improvements. *Journal of Applied Meteorology* **31**: 1359–1367.
Handoh IC, Bigg GR. 2000. A self-sustaining climate mode in the tropical Atlantic, 1995–1997: Observations and modelling. *Quarterly Journal of the Royal Meteorological Society* **126**: 807–821.
Handoh IC, Matthews AJ, Bigg GR, Stevens DP. 2006. Interannual variability of the tropical Atlantic independent of and associated with ENSO: Part II. The South tropical Atlantic. *International Journal of Climatology* DOI:10.1002/joc1342.
Hirst AC. 1988. Slow instabilities in tropical ocean basin-global atmosphere models. *Journal of Atmospheric Sciences* **45**: 830–852.
Hoskins BJ, Ambrizzi T. 1993. Rossby wave propagation on a realistic longitudinally varying flow. *Journal of Atmospheric Sciences* **50**: 1661–1671.
Hoskins BJ, Karoly DJ. 1981. The steady linear response of a spherical atmosphere to thermal and orographic forcing. *Journal of Atmospheric Sciences* **38**: 1179–1196.
Houghton RW, Tourre YM. 1992. Characteristics of low frequency sea-surface temperature fluctuations in the tropical Atlantic. *Journal of Climate* **5**: 765–771.
Huang B, Shukla J. 1997. Characteristics of the interannual and decadal variability in a general circulation model of the tropical Atlantic Ocean. *Journal of Atmospheric Sciences* **27**: 1693–1712.
Huang BH, Schopf PS, Pan ZQ. 2002. The ENSO effect on the tropical Atlantic variability: A regionally coupled model study. *Geophysical Research Letters* **29**: 2039, DOI: 10.1029/2002GL014872.
Joyce TM, Frankignoul C, Yang JY. 2004. Ocean response and feedback to the SST dipole in the tropical Atlantic. *Journal of Physical Oceanography* **34**: 2525–2540.
Jung T, Hilmer M, Ruprecht E, Kleppek S. 2003. Characteristics of the recent eastward shift of interannual NAO variability. *Journal of Climate* **16**: 3371–3382.
Kistler R, Kalnay E, Collins W, Saha S, White G, Woollen J, Chelliah M, Ebisuzaki W, Kanamitsu M, Kousky V, van den Dool H, Jenne R, Fiorino M. 2001. The NCEP-NCAR 50-year reanalysis: Monthly means CD-ROM and documentation. *Bulletin of the American Meteorological Society* **82**: 247–267.
Klein SA, Soden BJ, Lau NC. 1999. Remote sea surface temperature variations during ENSO: Evidence for a tropical atmospheric bridge. *Journal of Climate* **12**: 917–932.
Lau NC, Nash MJ. 1996. The role of the "atmospheric bridge" in linking tropical Pacific ENSO events to extratropical SST anomalies. *Journal of Climate* **9**: 2036–2057.
Liebmann B, Smith CA. 1996. Description of a complete (interpolated) outgoing longwave radiation dataset. *Bulletin of the American Meteorological Society* **77**: 1275–1277.
Liu Z, Zhang Q, Wu L. 2004. Remote impact on tropical Atlantic climate variability: statistical assessment and dynamic assessment. *Journal of Climate* **17**: 1529–1549.
Mariotti A, Ballabrera-Poy J, Zeng N. 2005. Tropical influence on Euro-Asian autumn rainfall variability. *Climate Dynamics* **24**: 511–521.
Marshall J, Kushnir Y, Battisti D, Chang P, Czaja C, Dickson R, Hurrell J, McCartney M, Saravanan R, Visbeck M. 2001. North Atlantic climate variability: phenomena, impacts and mechanisms. *International Journal of Climatology* **21**: 1863–1898.
Matthews AJ, Kiladis GN. 1999. Interactions between ENSO, transient circulation, and tropical convection over the Pacific. *Journal of Climate* **12**: 3062–3086.
Mehta VM. 1998. Variability of the tropical ocean surface temperatures at decadal-multidecadal timescales. Part I: The Atlantic Ocean. *Journal of Climate* **11**: 2351–2375.
Mo KC, Häkkinen S. 2001. Interannual variability in the tropical Atlantic and linkages to the Pacific. *Journal of Climate* **14**: 2740–2762.
Mo KC, Paegle JN. 2001. The Pacific–South American modes and their downstream effects. *International Journal of Climatology* **21**: 1211–1229.
Nobre P, Shukla J. 1996. Variations of sea surface temperature, wind stress, and rainfall over the tropical Atlantic and South America. *Journal of Climate* **9**: 2464–2479.
Okumura Y, Xie SP, Numaguchi A, Tanimoto Y. 2001. Tropical Atlantic air–sea interaction and its influence on the NAO. *Geophysical Research Letters* **28**: 1507–1510.

Copyright © 2006 Royal Meteorological Society

Peng S, Robinson WA, Li S. 2003. Mechanisms for the NAO responses to the North Atlantic SST tripole. *Journal of Climate* **16**: 1987–2004.
Peng S, Saravanan R, Ji L, Hegerl GC. 2000. The effect of local sea surface temperatures on atmospheric circulation over the tropical Atlantic sector. *Journal of Climate* **13**: 2195–2216.
Pozo-Vazquez D, Esteban-Parra MJ, Rodrigo FS, Castro-Diez Y. 2001. The association between ENSO and winter atmospheric circulation and temperature in the North Atlantic region. *Journal of Climate* **14**: 3408–3420.
Ruiz-Barradas A, Carton JA, Nigam S. 2000. Structure of interannual-to-decadal climate variability in the tropical Atlantic sector. *Journal of Climate* **13**: 3285–3297.
Ruiz-Barradas A, Carton JA, Nigam S. 2003. Role of the Atmosphere in climate variability of the tropical Atlantic. *Journal of Climate* **16**: 2052–2065.
Saravanan R, Chang P. 2000. Interaction between tropical Atlantic variability and El Niño-Southern Oscillation. *Journal of Climate* **13**: 2177–2194.
Spencer H, Slingo JM. 2003. The simulation of peak and delayed ENSO teleconnections. *Journal of Climate* **16**: 1757–1774.
Sutton RT, Jewson SP, Rowell DP. 2000. The elements of climate variability in the tropical Atlantic region. *Journal of Climate* **13**: 3261–3284.
Sutton RT, Norton WA, Jewson SP. 2001. The North Atlantic Oscillation-What role for the Ocean? *Atmospheric Science Letters* **1**: 89–100 DOI: 10.1006/asle.2000.0018.
Tourre YM, Rajagopalan B, Kushnir Y. 1999. Dominant patterns of climate variability in the Atlantic Ocean during the last 136 years. *Journal of Climate* **12**: 2285–2299.
Tseng L, Mechoso CR. 2001. A quasi-biennial oscillation in the equatorial Atlantic Ocean. *Geophysical Research Letters* **28**: 187–190.
Wu AM, Hsieh WW. 2004. The nonlinear association between ENSO and the Euro-Atlantic winter sea level pressure. *Climate Dynamics* **23**: 859–868.
Xie SP, Carton JA. 2004. Tropical Atlantic variability: Patterns, mechanisms, and impacts. In *Earth Climate: The Ocean–Atmosphere Interaction*, Wang C, Xie SP, Carton JA (eds). Geophysical Monograph. AGU: Washington, DC.
Xie SP, Philander SGH. 1994. A coupled ocean–atmosphere model of relevance to the ITCZ in the central Pacific. *Tellus* **46A**: 340–350.
Xie SP, Tanimoto Y, Noguchi H, Matsuno T. 1999. How and why climate variability differs between the tropical Atlantic and Pacific. *Geophysical Research Letters* **26**: 1609–1612.
Zebiak SE. 1993. Air–sea interactions in the equatorial Atlantic region. *Journal of Climate* **6**: 1567–1586.

Copyright © 2006 Royal Meteorological Society